Ore Geology Reviews 87 (2017) 71–87

Contents lists available at ScienceDirect

Ore Geology Reviews

journal homepage: www.elsevier.com/locate/oregeorev

Continuous growth of hydrogenetic ferromanganese crusts since 17 Myr ago on Takuyo-Daigo Seamount, NW Pacific, at water depths of 800–5500 m

Akira Usui [a,*], Keisuke Nishi [a], Hisaaki Sato [a], Yoshio Nakasato [a], Blair Thornton [b], Teruhiko Kashiwabara [c], Ayaka Tokumaru [d], Aya Sakaguchi [e], Kyoko Yamaoka [f], Shingo Kato [c], Shota Nitahara [g], Katsuhiko Suzuki [c], Koichi Iijima [c], Tetsuro Urabe [h]

[a] Center for Marine Core Research Institute, Kochi University, Japan
[b] Institute for Industrial Science, University of Tokyo, Japan
[c] R & D Center for Marine Resources, JAMSTEC, Japan
[d] Metals Exploration Dept., JOGMEC, Japan
[e] Division of Chemistry, Tsukuba University, Japan
[f] Geological Survey of Japan, National Inst. Advanced Industrial Science and Technology (AIST), Japan
[g] Tokyo University of Pharmacy and Life Sciences, Japan
[h] Emeritus Professor, University of Tokyo, Japan

ARTICLE INFO

Article history:
Received 13 April 2016
Received in revised form 25 September 2016
Accepted 26 September 2016
Available online 29 September 2016

Keywords:
Ferromanganese crust
Oxygen minimum zone (OMZ)
Northwest Pacific
Takuyo-Daigo
Seamount
Hydrogenetic
Outcrop
Marine minerals
International Seabed Authority/United Nations (ISA/UN)
Paleoceanography
Remotely operated underwater vehicle (ROV)

ABSTRACT

Ferromanganese crusts cover all outcrops on Takuyo-Daigo seamount traversed during remotely operated underwater vehicle (ROV) dives, except in places covered by foraminifera sand. Takuyo-Daigo is a Cretaceous seamount located in the northwest Pacific Ocean. Geological and bathymetric mapping provide the framework for this study. Chemical and mineralogical analyses of the hydrogenetic ferromanganese crusts show temporal and spatial variations typical of those found in previous studies. Outcrops from 800 to 5500 m water depths are covered with ferromanganese crusts up to 105 mm thick. Beryllium isotope dating shows that the crusts have apparently been growing continuously at all water depths, even through the modern oxygen minimum zone (OMZ), contrary to some earlier models for deposition. Growth rates vary from 2.3 to 3.5 mm/Myr, with Fe or Mn fluxes of 0.07–0.11 g/cm^2/Myr since the early-middle Miocene. Co/Mn ratios decrease with water depth while Fe/Mn and other metallic elements increase or show no change, based on the analysis of the uppermost crust surface. This is probably because Co is the most abundant redox-sensitive element derived from seawater that occurs in crusts.

1. Introduction

Northwest Pacific offshore seamounts are expected to be future marine mining sites for ferromanganese (Fe-Mn) crusts, which contain metals necessary for high-tech industries (Hein et al., 2013), such as Co, Ni, Te, Ti, Pt, and rare earth elements (REEs). These crusts are archives of climate and ocean history (e.g. Bayon et al., 2004; Halliday et al., 1998; Koschinsky et al., 1996). However, little is known about their small-scale distribution patterns, mineral diversity and variability, and genetic controls, because of the lack of high-resolution mapping and comparative analyses from various crust deposits (Suave et al., 1989; Glasby, 2000). Hydrogenetic Fe-Mn crusts are condensed stratigraphic sections that have accumulated over millions of years, precipitating from changing compositions of seawater and environment. Comprehensive studies have been lacking, but are critical to more fully understand crust genesis on regional, local, and outcrop scales (Glasby et al., 2007; Hein et al., 2000).

On-site geological observations and microscopic, geochemical, and mineralogical analyses are essential for discussing the depositional processes and environments, as well as for exploration and economic evaluation. Previous manned-submersible and ROV dives have shown a common occurrence of Fe-Mn crusts and bio-diversity on seamounts (Templeton et al., 2009; Schlacher et al., 2014), but only limited

* Corresponding author.
E-mail address: a-usui@kochi-u.ac.jp (A. Usui).

http://dx.doi.org/10.1016/j.oregeorev.2016.09.032
0169-1368/

geological results have been published. Our team, comprising geologists, mineralogists, geochemists, physical engineers and microbiologists, utilized remotely operated underwater vehicles (ROVs) for in situ measurements, observations, and sampling of undisturbed and uncontaminated Fe-Mn crusts at a model seamount, the Takuyo-Daigo seamount (Figs. 1 and 2). The seamount is located within the Japanese Exclusive Economic Zone (100 nm from the Minami-Torishima Island, or Marcus Island) in the northwest Pacific (Fig. 2), and only 300 nm from Japan's licensed area for exploration of Co-rich Fe-Mn crusts under the International Seabed Authority. In 2009, the first Japanese ROV geological survey of Fe-Mn crusts was successfully completed with Hyper-Dolphin 3K of the Japan Agency for Marine-Earth Science and Technology (JAMSTEC) at the Takuyo-Daigo seamount (Usui et al., 2011). The ROV cruises to nearby seamounts (Usui et al., 2013) utilized this powerful and efficient tool for seafloor observation and delicate sampling of crusts. A total of 25 ROV dives of the Hyper Dolphin 3K/4K ROV and the Kaiko Mark IV ROV provided excellent seabed views, fine-scale seabed features, and tightly controlled samples for analyses, rather than using a chain-bag dredge, manned submersible, or remotely operated drill (Table 1; Fig. 3). Undisturbed and continuous sampling over five tracks was achieved with a continuous seabed observation with 2–3 m altitude during the R.V. Natsushima Cruise NT09-02 from the southernmost ridge of Takuyo-Daigo seamount, collecting >1 ton of crust material at about 110 sites along approximately a total of 10 km of lines. In addition, real-time monitoring of position, water depth, temperature, salinity, and dissolved oxygen was achieved, and most samples were found to be suitable for millimeter-scale compositional analyses and stratigraphic and magnetostratigraphic laboratory measurements. The intact surface of the crust material, collected without any abrasion and breakdown, was also valuable for microbiological study and structural characterization of surface precipitates.

These studies enabled us to produce a paleoceanographic reconstruction essential for reliable mineral exploration and resource estimate. This is the first successful geological mapping effort using ROV for Fe-Mn crusts, which can be used as a standard method for characterizing hydrogenetic Fe-Mn crust deposits at offshore seamounts.

Our team addressed the following objectives: 1) to characterize the mode of distribution of Fe-Mn crusts on the substrate rocks, and relationships to microtopography and geology; and 2) to understand the growth processes and depositional history of critical metals over the last 10–15 Myr.

2. Geological setting and background

The tectonic theory of mantle plumes suggests that a large number of seamounts and plateaus were formed during the course of intensive upwelling from the Earth's interior during the Cretaceous (85–150 Ma) (Nakanishi et al., 1999; Koppers et al., 2003). Plume convection also formed the hotspot seamount chains between the East Pacific Rise and the northwest Pacific margins, which is a major island-arc system (Fig. 1) (Davis and Pribac, 1997; Koppers et al., 2003). The northwestern Pacific seafloor is characterized by the complex morphology of abundant and huge seamounts, where extensive hydrogenetic Fe-Mn crusts commonly occur (Glasby et al., 2007). The age of these seamounts ranges from Middle to Late Cretaceous. The seamounts and guyots (flat-top seamounts) in the modern northwestern Pacific formed at 10–20°S in the southern hemisphere during the Cretaceous period (Nakanishi and Winterer, 1998), many of which traversed the equator as carbonate reefs followed by subsidence (Larson and Freymueller, 1995; Winterer et al., 1993).

These seamounts are roughly of the same age as the oceanic crust (Koppers et al., 1998, 2003), which ranges from the Late Jurassic to the Late Cretaceous, with age increasing from the seamounts of the Marshall Islands toward the northwest. The Takuyo-Daigo seamount is a member of the North Wake hotspot chain, dated to be between 100 and 120 Myr (Koppers et al., 2003; Tokumaru et al., 2015). Although most seamounts formed during the Cretaceous, younger seamounts formed by hotspots are also distributed across part of the area (Fig. 2).

The thick hydrogenetic Fe-Mn crusts in the mid-Pacific seamounts were first described by German geologists in the 1980s (Halbach et al., 1983; Halbach and Puteanus, 1984). The crusts and nodules are expected to grow unless there is rapid biogenic sedimentation, mass wasting, or tectonic movement (Usui and Someya, 1997; Hein et al., 2000; Usui and Okamoto, 2010; Okamoto and Usui, 2014). Similar analyses have also been conducted for manganese deposits from various areas in the northwestern Pacific (e.g., Usui et al., 1994; Jeong et al., 2000;

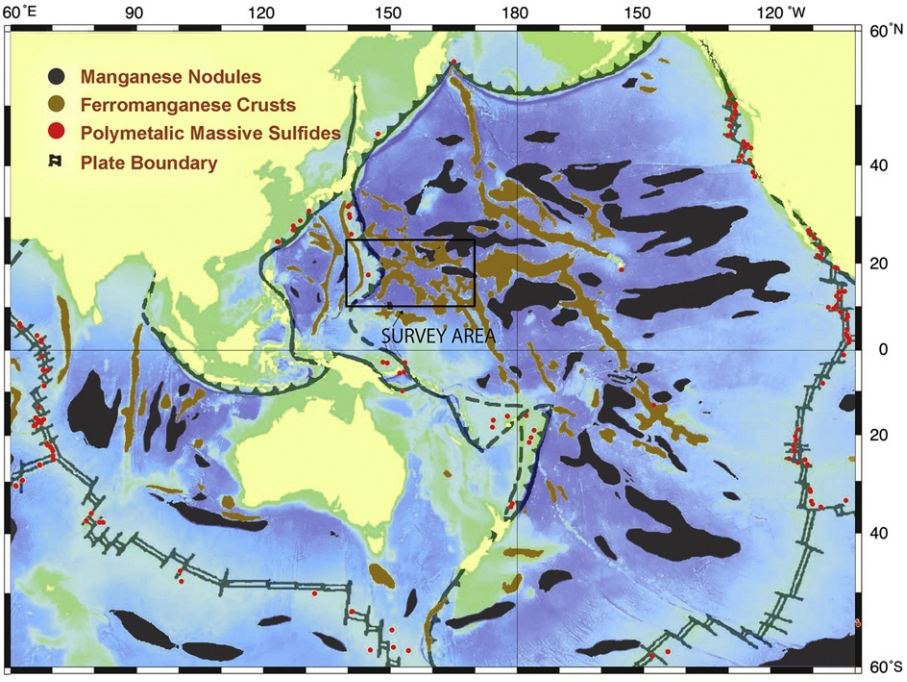

Fig. 1. Distribution of marine minerals of the Pacific.
Modified from Usui (2010).

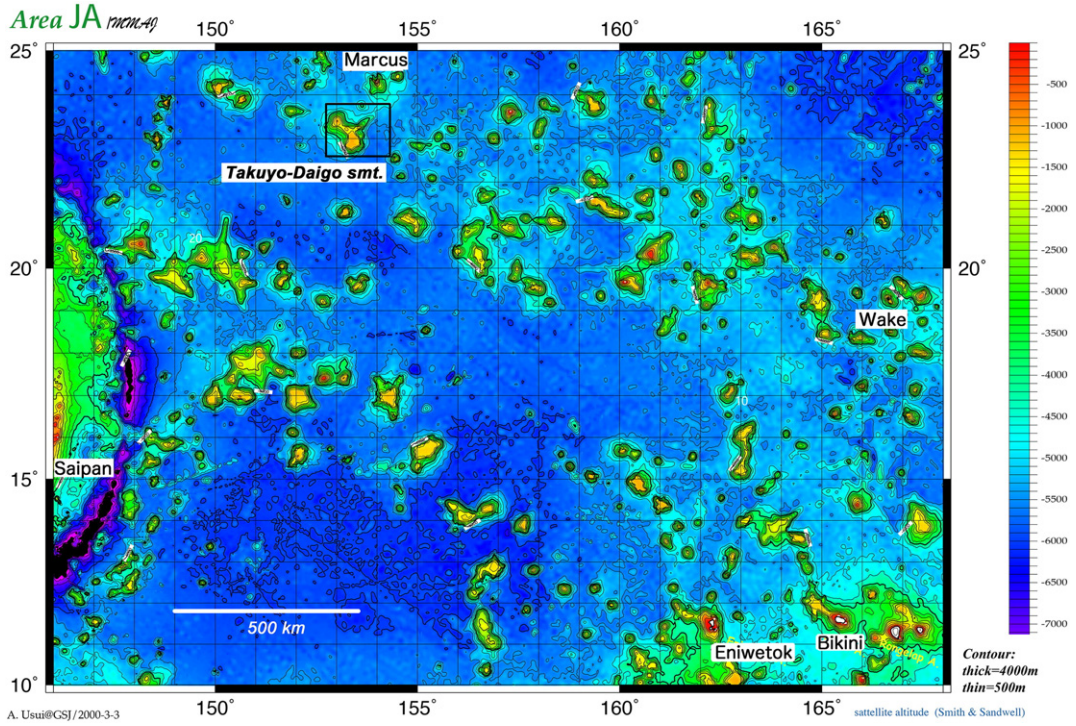

Fig. 2. Index map of study area, Takuyo-Daigo seamount and adjacent seamounts on ETOPO5-based bathymetric map.

Usui et al., 2007; Hein et al., 2012), but the general mode of occurrence and patterns of regional and small-scale variations are yet to be well characterized. Further details of age, minor element variation, and relationship to geological environments are not well known at present.

Takuyo-Daigo is a large guyot, about 100 km across, which was selected as a model area for geoscientific study by the Japanese organizations (JAMSTEC, JOGMEC, Universities of Tokyo, and Kochi). Most of the flat top is thinly covered with young foraminiferal ooze, though this ooze is minimal or lacking on the shoulders and slopes. The top of the seamount is a small volcanic pinnacle at about 850 m water depth. The steepest slopes of about 20–25° encircle the margin of the flat top. The topography of the slopes indicates frequent mass wasting on the flanks of the seamount after subsidence.

Like other nearby seamounts in the northwest Pacific (Winterer et al., 1993; Glasby et al., 2010), the Takuyo-Daigo seamount may have started as a Cretaceous large-scale composite volcano island, which was wave-eroded at sea level, and after reef-building, isostatic subsidence submerged the flat-topped volcanic edifice. The steep shoulders and slopes serve as stable outcrops for the growth of the Fe-Mn crusts. A very flat substrate prevailing near the margins of the flat top of Takuyo-Daigo is the wave-eroded terrace of a Cretaceous rudist reef (Yasuo Kondo, University of Kochi and Shinichi Sano, Fukui Prefectural Dinosaur Museum, Japan, unpublished, pers. comm. 2013). This occurrence simply indicates that the seamount subsidized in the Cretaceous or later. Such stable outcrops do not accumulate sediment on the slopes, which permits growth of the crusts. On the other hand, rapid biogenic sedimentation and mass wasting inhibit growth.

3. Methods of on-site observation and sampling with ROV

Twenty-five ROV dives were carried out on the tops, shoulders and flanks of the seamount, while five dives were centered along a total 10-km-long survey line at a southern flank on Takuyo-Daigo seamount with Hyper-Dophin at depths above 3000 m (Table 2; Fig. 3). Deeper seabeds were in places surveyed with Kaiko below 3000 m. The principal environmental parameters of temperature, salinity, and dissolved oxygen were continuously measured from the sea surface to the bottom and along all survey tracks of the ROVs. In advance of the ROV dives, we conducted a multi-narrow-beam bathymetric study between the water depths of 800 and ~6000 m.

The ROV observation and sampling of Fe-Mn crusts proved an efficient means of on-site mapping over areas of rugged and variable microtopography (Usui et al., 2011). Such on-site ROV mapping and sampling is also valuable for resource evaluation. Our successful results from these cruises suggest that no other methods, such as dredging, deep-tow TV/cameras, compact drills, or acoustic probes, are better than ROV mapping for these purposes.

We carried out 18 ROV dives using the HyperDolphin 3K, and more recently seven dives with a new ROV, Kaiko Mark IV (both owned by JAMSTEC, Yokosuka) at the Takuyo-Daigo seamount. The earlier bathymetric results indicated acoustic high reflection from rock outcrops and steep (>15–20° gradient) seafloors, but cannot always define the distribution of the Fe-Mn crusts. The ROVs are equipped with a <10-m-precision SSBL positioning system, CTD-DO sensors, sonars, 7-joint powerful manipulators (>400 kgf grip), push cores, a

Table 1
Cruises of ROV dives for ferromanganese crusts.

Cruise	Date	Ship	ROV	Area	ROV dives	Dive number	Range (water depth)	Chief sci.
NT09-02	Feb 2009	Natasushima	HyperDophin 3K	Takuyo-Daigo (South-West)	7	#953–#959	953 m–2996 m	Urabe, T.
NT10-11	Jun 2010	Natasushima	HyperDophin 3K	Takuyo-Daigo (South)	3	#1144–#1146	1152 m–2888 m	Thornton, B.
NT12-05	Dec 2012	Natasushima	HyperDophin 3K	Takuyo-Daigo (North-Center)	3	#1352–#1354	1429 m–2900 m	Thornton, B.
NT13-13	Jun 2013	Natasushima	HyperDophin 3K	Takuyo-Daigo (South)	5	#1540–#1544	1420 m–1697 m	Thornton, B.
KR16-01	Jan 2016	Kairei	Kaiko Mark IV	Takuyo-Daigo (South)	7	#678–#684	1100 m–5500 m	Iijima, K.

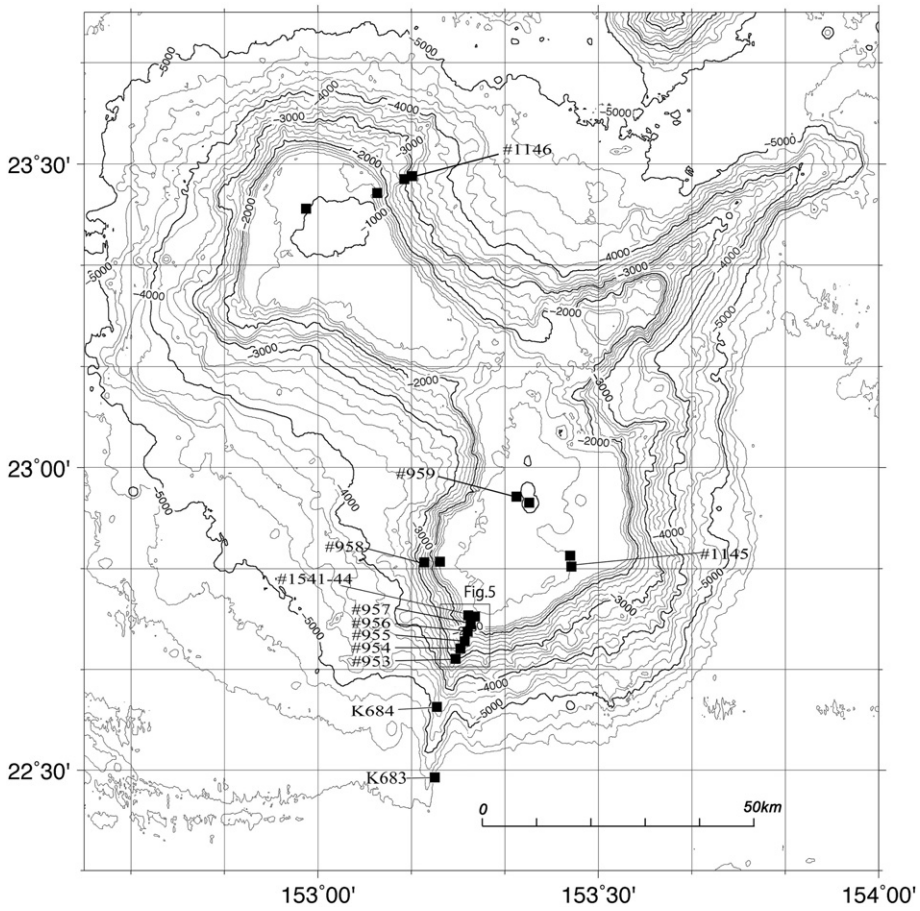

Fig. 3. Topography of the Takuyo-Daigo seamount. Small solid squares are sampling sites. # and K means ROV Hyper-Dolphin and Kaiko (JAMSTEC) respectively. Sampling was not continuous over the entire water depth of the seamount flanks, with the deepest site at 5500 m, then 4200 m, and continuous sampling lines from 3000 to 1200 m consisting of 110 sampling sites.

Niskin water sampler, hi-vision TV cameras and the newly innovated "acoustic crust-thickness sensor" which indicates continuously the possible boundary between the substrate and crusts with sensors equipped with a ROV, whose first report was published elsewhere (Thornton et al., 2013). The sampling intervals for crusts were about 100–200 m water depth. The observations were conducted while scanning the seafloor with a TV camera at an altitude of 2–5 m above the seafloor, at a speed of ~1 kt (0.5 m/s) or less. Undisturbed samples taken by the manipulator and rotary blade cutter enabled us to characterize the compositional variations with water depth along the continuous survey lines along the slopes.

4. Methods of chemical, mineralogical, and chronological analyses

We used a reflecting microscope on polished sections and a microfocus X-ray fluorescence (XRF) analytical microscope (HORIBA XGT-7200 V) at the Kochi University for a microstratigraphic description of texture and compositional features. We can demonstrate the apparent temporal variations in major (Mn and Fe) and minor elements, as well as in major and detrital mineral components and biogenic materials. These methods constructed the most important framework for characterizing the crusts as archives for paleoenvironmental conditions, and in consideration of growth history and metal cycling.

We analyzed general mineralogy using X-ray diffraction (Multiflex, Rigaku). The surface of each crust and each section at 3-mm intervals were taken from the stratigraphic column of each crust sample for chemical analysis. The chemical analysis (ICP-OES) was conducted after closed-chamber digestion of air-dried powders for major metallic elements (Fe, Mn, alkali, alkali earth, Ni, Co, Cu, Pb, Al, Ti, Zn, V, Y, S, and P) using four acids (hydrofluoric, hydrochloric, nitric, and perchloric) at the Ontario Geological Survey (Toronto, Canada). ICP-MS was used for most minor and trace elements, such as Ba, Be, Bi, Cd, Cs, Ga, Gd, Hf, In Li, Nb, Sc, Sr, Ta, Tm, W, Cr, REE, U, and Th (Table 3). The manganese nodule reference sample JMn-1 was used for correction of the chemical analyses.

Beryllium isotope separation and acceleration mass spectrometer (AMS) isotope analyses were undertaken at the Institute of Geological and Nuclear Science (GNS), New Zealand by I. Graham, A. Zondervan, and R. Ditchburn. The $^{10}Be/^{9}Be$ dating was performed at ~1 cm intervals on 23 portions of the section from five crust samples (Table 4). The Be isotope analytical methods were described by Graham et al. (2004). We use here a modern seawater $^{10}Be/^{9}Be$ ratio of 1.289×10^{-7} (von Blanckenburg and Bouchez, 2014) and a half-life of 1.387 Ma (Oda et al., 2011; Korschinek et al., 2010) for the calculations. We verified the Be dating with a paleomagnetic method (Oda et al., 2011; Noguchi et al. 2017). Here we assume that the oldest measured Be isotope age measured by this method is about 12 Myr (middle Miocene), with extrapolated ages back to 17 Myr (for details see Nishi et al., 2017).

We used a parameter for metal flux (mass accumulation rate) for hydrogenetic Fe-Mn crusts similar to that used for sediment cores (Puteanus and Halbach, 1988; Manheim and Lane-Bostwick, 1988), defined as MF ($mg/yr/cm^2$) = C (concentration on air-dried samples) × D (dry density) × R (growth rate determined using Be isotopes). The mass flux determines the rate of fixation of an element to the crust, instead of simply the rate of growth, which can be used to show variations in time and space at millimeter-scale intervals within crusts.

Table 2
Samples used for chemical and mineralogical description.

Dive no.	Sample no.	Depth (m)	Latitude	Longitude (E)	Occurrence	Column no.	Weight on site	Size (cm)	Name	Thickness of crust	Substrate	Remarks
HPD#953-	R-02	2987	22°40.995′ N	153°14.609′E	Outcrop	A (n = 11)	17 kg	35 × 35 × 17	Crust	38 mm	Calcareous conglomerate	Medium thick, typical smooth surface crusts. Much less abundant organisms on surface than those from shallower depths. Cross section shows monotonous structure of earthy black compact layers. Taken by rock saw from the rock outcrop.
HPD#954-	R-10	2239	22°42.453′N	153°15.418′E	Outcrop	B (n = 13)	2.1 kg	21 × 14 × 6	Crust	35 mm	Calcareous conglomerate	Medium thick, typical smooth surface crusts. Less abundant organisms on surface than those from shallower depths. Cross section shows monotonous structure of earthy black two compact layers. Taken by rock saw from the rock outcrop.
HPD#956-	R-15	1440	22°44.601′N	153°15.991′E	Roll (slab)	C (n = 23)	15 kg	41 × 31 × 12	Slab	80 mm	Calcareous sandstone	Flat 10 cm thick crust fragment. Typical dual structure on section and knobby surface structure. Columnar growth is characteristic on the section. Total thickness is the greatest in this depth range. Taken by manipulator from seafloor.
HPD#958-	R-12	1424	22°50.437′N	153°12.893′E	Roll	E (n = 21)	30 kg	78 × 35 × 9	Slab	90 mm	Calcareous sandstone	Similar to the sample above. Taken by manipulator from seafloor.
HPD#959-	R-11	965	22°56.483′N	153°22.103′E	Roll	F (n = 10)	4.1 kg	25 × 19 × 10	Boulder nodule	35 mm	Hydrothermal manganese ox.	Knobby surface and earthy black columnar growth layers are typical. The youngest upper layer entirely covers a fragment of the crust. Substrate is of typical hydrothermal manganese oxide. Taken by manipulator from seafloor.

5. Results and discussion

5.1. On-site observation of occurrence and distribution of ferromanganese crusts

The on-site observation and geological mapping of the seabed using ROVs allow us to collect high-quality geological samples of undisturbed stratigraphic sections of the crusts and the underlying substrate rock, and to characterize the crust surfaces as growing modern precipitates. The undisturbed samples taken from the outcrops enabled us to describe the small-scale variation across the entire flank as well as to determine microscopic surficial and internal compositional variations (Fig. 3 and Table 2). The ROV dives are focused along a 30-km-long ridge on the southern side of the seamount from the foot to the top of the seamount. Entire outcrops of hard substrate and large boulders of volcanic rocks and calcareous rocks are covered with 10 to 100-mm-thick Fe-Mn crusts, whereas thick foraminifera sands cover mostly the flat tops at depths between 850 and 1000 m (Figs. 4–6). The surface of the crusts over the slopes at depths below 1100 m, is scarcely and thinly covered with foraminifera sand. Flat terraces and depressions are commonly filled with the sediments that bury the crusts. On the flat tops, manganese nodules or large boulders coated with Fe-Mn oxides are often distributed where sediments are thinner. On TV images we often observe evidence of sediment chutes.

Our small-scale mapping reveals a clear relationship of the morphology of the crusts with basement geology, microtopography, and probably with oceanographic and sedimentary processes. Outcrops at water depths between 1200 m and 5500 m (average 10–12° gradient) are covered with crusts showing a maximum thickness of 105 mm (Figs. 5 and 6). The thickness is variable, but we do not see outcrops without crusts from any site along the survey lines. The thickest crusts occur near the summit margin and somewhat below it (1200–2400 m water depths), although the local variation is considerable. Flat (low gradient) summit areas and terraces are usually covered with thicker calcareous sediments, but host some hydrogenetic Fe-Mn nodules. In the survey line on the south flank ridge (Fig. 6), thick crusts are usually associated with steep (>15° gradient) outcrops of volcanic rock, and thinner crusts with a less steep knobby substrate composed of consolidated debris flow (calcareous conglomerate). This indicates that the seafloor morphology and geology of the substrate are closely related to the growth of hydrogenetic Fe-Mn crust deposits. This occurrence of thick Fe-Mn crusts on the seamount may have been controlled essentially by sedimentary conditions during and after the subsidence of the seamount. Surface morphology (flat, knobby, gritty) is apparently related to water depth, showing smoother growth texture on deeper outcrops (Fig. 7).

5.2. Compositional variability in time and space

The Takuyo-Daigo seamount crusts contain a maximum of 1.1% cobalt, 0.5% nickel, and 0.2% total REE (Table 3). The secular distributions of metals show considerable variation, but have similar patterns with water depth (from 3000 to 900 m), indicating similar paleoenvironmental conditions during the formation since about 17 Ma (Fig. 8; See next section).

Mineralogical description and XRF data suggest that apparent banding, such as alternation of dense/black and porous/brownish layers, is principally due to the microstructure of the crusts and the abundance of detrital particles, and not due to concentrations of metal oxides (Fig. 9). Thus, correlations based on visible characteristics among stratigraphic columns of Fe-Mn crusts are often poor because of localized (detrital, volcanogenic and biogenic) sources of mineral particles. The chemical properties of metals in the hydrogenetic iron and manganese components are more important in discussing relationships to regional and global environments. The secular element profiles in the Fe-Mn crusts from two different water depths on Takuyo-Daigo

Table 3
Chemical composition of top surface (<1 mm) of the crust sample (in ppm to air-dried basis).

Local #	Sample	Water depth (m)	Al	Ca	Co	Cu	Fe	K	Mg	Mn	Na	Ni	P	Pb	S	Sr	Ti	V	Y	Zn	Ce	La	Pr	Ba	Be	Bi
V01	HPD#953-R01	2991	5820	23,800	4700	360	176,000	3910	7400	187,000	13,100	2400	3700	1370	2130	1120	7200	530	140	450	1050	250	60	840	3.0	29
V04	HPD#953-R06	2952	5570	21,600	5400	350	157,000	3830	7200	185,000	13,800	2700	3300	1360	2290	1080	7500	500	130	440	990	230	58	810	3.2	27
V05	HPD#953-R12	2940	6180	22,100	4800	340	160,000	4030	7200	172,000	15,100	2300	3500	1300	2330	1060	7300	490	130	420	1040	230	58	830	2.9	28
V06	HPD#953-R15	2892	4890	21,400	5800	320	151,000	3760	7400	192,000	13,900	3100	3200	1330	2520	1120	7600	500	140	430	1000	270	65	800	3.1	29
V09	HPD#953-R20	2736	5310	21,300	4600	280	158,000	3630	6900	177,000	13,600	2600	3400	1310	2260	1060	6600	500	140	420	990	260	62	840	3.7	28
V12	HPD#953-R23	2618	4690	24,700	5000	280	158,000	3620	7600	185,000	14,400	2700	3600	1340	2580	1120	6900	520	130	440	940	240	59	840	3.3	28
V14	HPD#954-R01	2601	5190	23,800	5000	270	161,000	3720	7200	184,000	14,100	2500	3600	1330	2400	1100	6800	510	140	430	960	260	61	800	2.8	27
V15	HPD#954-R03	2516	5420	25,400	5000	270	160,000	3690	7200	181,000	13,500	2500	3600	1300	2330	1090	6700	500	140	420	930	250	58	830	2.8	27
V18	HPD#954-R06	2411	5760	27,300	5200	240	152,000	3670	7100	172,000	14,000	2500	3500	1290	2430	1070	7000	460	130	400	980	250	57	840	2.9	25
V19	HPD#954-R09	2313	5320	25,300	4400	260	161,000	3580	7000	175,000	12,900	2500	3800	1380	2280	1100	6400	520	140	430	930	250	58	820	2.8	25
V20	HPD#954-R10	2239	5260	28,300	5400	230	152,000	3610	7200	190,000	12,700	3100	3600	1320	2210	1120	6500	510	140	440	860	250	58	810	3.0	26
V21	HPD#955-R04	2209	5630	27,600	5200	260	154,000	3830	7200	187,000	14,600	3000	3700	1350	2490	1120	6500	510	140	450	880	260	60	850	3.0	27
V22	HPD#955-R08	2093	5520	29,300	5300	250	149,000	3680	7000	175,000	13,300	2900	3700	1350	2290	1110	6800	480	140	420	940	260	59	850	2.6	27
V23	HPD#955-R09	2008	5730	26,800	5300	240	155,000	3950	7300	191,000	15,400	3100	3600	1360	2570	1120	6400	500	140	420	860	270	60	860	3.4	26
V25	HPD#955-R12	1937	6220	25,700	5100	220	122,000	4120	7400	174,000	14,800	3000	3900	1430	2640	1140	6000	520	150	440	850	240	54	800	2.3	25
V26	HPD#956-R03	1907	8010	28,800	5100	230	123,000	4600	7200	170,000	15,200	2500	3800	1400	2570	1110	5900	500	140	420	850	240	52	830	2.3	23
V27	HPD#956-R06	1834	7590	21,200	5300	260	125,000	4410	7400	170,000	14,700	2900	3800	1540	2540	1100	6900	500	140	460	860	240	52	860	2.3	23
V28	HPD#956-R09	1626	6070	18,300	5900	190	125,000	4230	7400	193,000	14,500	3100	4100	1670	2680	1170	6600	570	160	440	900	270	56	790	2.7	24
V29	HPD#956-R11	1472	5290	18,700	6900	160	122,000	4010	7600	202,000	14,700	3200	4300	1800	2850	1200	5900	600	160	450	920	260	55	760	2.5	24
V30	HPD#956-R13	1448	5860	18,000	6600	150	126,000	4070	7400	195,000	15,100	2800	4400	1810	2760	1190	5800	590	160	420	950	260	54	750	2.6	25
V32	HPD#956-R15	1440	5010	18,000	6100	140	124,000	3700	7000	193,000	14,500	2700	4400	1780	2670	1170	5400	600	160	420	970	260	55	770	3.3	25
V36	HPD#956-R08	1293	5420	17,200	7700	200	117,000	3830	7500	202,000	14,500	3300	4100	1910	2750	1170	5600	580	150	430	1000	260	52	860	3.1	26
V38	HPD#956-R11	1252	3800	17,900	8800	150	115,000	3700	7700	221,000	15,500	4200	4300	1970	2940	1200	5500	620	160	460	930	250	52	770	2.7	28
V39	HPD#956-R15	1207	4360	17,800	7800	160	119,000	3460	7200	201,000	11,700	3100	4500	1930	2260	1200	5400	620	160	420	970	250	52	740	2.7	28
V42	HPD#958-R02	1923	8320	17,500	4500	600	123,000	4440	7700	180,000	14,300	3400	3500	1630	2510	1120	6800	520	130	520	870	210	44	960	3.0	31
V43	HPD#958-R04	1838	6850	18,000	4600	200	133,000	4310	7300	182,000	14,500	2800	4100	1650	2610	1180	5700	570	160	450	830	270	56	850	3.1	23
V44	HPD#958-R06	1600	4630	17,300	7300	160	120,000	3760	7100	199,000	14,400	3300	3800	1700	2690	1150	7800	520	150	440	1050	260	54	770	2.5	20
V49	HPD#958-R05	1057	3730	18,000	11,200	160	107,000	3600	7800	219,000	15,100	3400	4200	2090	2830	1170	5500	620	150	440	920	250	53	740	2.7	32
V51	HPD#958-R07	1019	3090	17,900	8800	160	106,000	3270	7300	199,000	14,200	3100	4300	2000	2790	1150	4800	630	150	410	810	240	50	680	2.4	30
V52	HPD#958-R11	965	3340	18,800	10,600	170	109,000	3510	7700	215,000	15,200	3200	4500	2170	2990	1190	5000	650	160	430	780	250	53	760	2.4	35
V53	HPD#958-R15	950	6370	17,800	8800	260	115,000	3760	9000	202,000	14,600	3600	4700	2080	2760	1150	5100	640	160	490	940	230	47	730	2.9	31
V55	HPD#958-R18	953	4580	17,800	10,900	310	100,000	3840	9200	230,000	15,100	5400	4000	2050	2830	1120	5000	610	140	530	870	220	46	800	2.5	33
V58	MT702-AD02	1600	4440	17,000	5300	180	119,000	3520	7100	187,000	12,700	3200	4000	1790	2680	1140	5100	600	150	470	790	250	52	800	3.3	24
V59	MT471-AD01	3794	9580	14,100	2900	430	165,000	4530	6500	141,000	11,800	1500	3200	1480	1770	990	6800	490	130	420	1250	250	60	920	3.2	27
V60	MT703-AD03	1774	5870	19,100	5300	160	127,000	3890	6900	170,000	14,000	2800	4400	1670	2400	1120	5900	540	150	430	1010	240	51	770	2.6	27

Table 3 (*continued*)

Local #	Cs	Dy	Er	Eu	Ga	Gd	Hf	Ho	In	Li	Lu	Nb	Nd	Pr	Sc	Sm	Sn	Ta	Tb	Th	Tm	U	W	Yb	Zr	ΣREE
V01	0.57	50	25	14	4.9	57	5.7	9.2	0.29	2.8	3.2	30.6	255	60	8.9	56.9	3.41	0.46	8.5	23.1	3.6	11.6	36.7	22.0	424	1860
V04	0.56	48	24	13	6.0	55	5.0	8.9	0.33	3.1	3.1	31.5	243	58	9.3	54.4	3.50	0.48	8.2	9.4	3.4	11.0	41.4	21.0	393	1760
V05	0.66	47	24	13	6.2	55	5.8	8.8	0.30	3.3	3.0	33.2	247	58	9.5	55.3	3.45	0.47	8.2	16.1	3.3	11.1	34.0	20.7	440	1810
V06	0.54	51	26	14	6.0	59	4.3	9.6	0.34	2.6	3.4	29.2	269	65	9.1	60.0	3.62	0.47	8.9	43.8	3.7	11.1	47.5	22.8	337	1860
V09	0.53	51	26	14	4.0	58	5.2	9.6	0.30	3.0	3.3	32.6	262	62	10.8	58.5	2.70	0.44	8.8	42.1	3.7	11.4	42.1	22.5	432	1820
V12	0.52	49	25	14	4.8	56	4.6	9.2	0.30	2.8	3.2	29.4	253	59	10.4	56.4	3.42	0.40	8.4	8.5	3.6	11.2	39.9	21.8	392	1730
V14	0.51	48	25	14	4.8	57	5.1	9.1	0.29	2.6	3.2	29.5	256	61	8.8	57.1	3.21	0.41	8.4	43.5	3.5	11.0	37.0	21.9	405	1780
V15	0.54	47	24	13	5.0	55	5.2	9.0	0.29	2.7	3.1	29.8	246	58	8.7	54.4	2.89	0.40	8.2	40.6	3.4	11.0	36.5	21.2	415	1720
V18	0.56	46	24	13	4.2	53	5.8	8.7	0.30	3.3	3.0	33.4	240	57	9.0	53.4	2.75	0.43	7.9	46.4	3.4	10.8	34.7	20.8	454	1760
V19	0.47	48	25	13	4.4	55	5.5	9.2	0.27	2.8	3.2	32.1	246	58	9.0	53.9	3.42	0.38	8.2	37.0	3.5	11.3	37.7	21.8	448	1720
V20	0.49	49	25	13	4.6	56	4.7	9.3	0.29	2.8	3.2	29.3	244	58	9.3	54.0	1.62	0.37	8.3	30.0	3.6	11.3	42.7	22.0	407	1650
V21	0.55	50	26	13	5.0	56	5.0	9.5	0.29	3.0	3.4	30.6	252	60	9.6	55.5	1.65	0.39	8.4	40.7	3.7	11.6	43.7	23.0	416	1700
V22	0.55	49	26	13	4.8	56	6.0	9.4	0.31	2.9	3.3	33.6	248	59	8.1	54.8	1.97	0.44	8.3	44.4	3.6	11.9	40.2	22.7	434	1750
V23	0.60	49	26	13	4.7	56	5.6	9.5	0.31	3.5	3.4	35.8	254	60	9.8	55.0	1.78	0.39	8.4	39.9	3.7	11.6	47.8	22.7	476	1690
V25	0.57	47	25	12	3.3	53	5.9	9.1	0.28	2.9	3.3	32.6	231	54	7.2	50.3	4.00	0.41	8.0	43.4	3.5	11.6	39.0	22.1	402	1600
V26	0.81	45	24	12	3.5	52	6.2	8.7	0.27	3.3	3.1	34.8	224	52	6.7	48.6	4.08	0.43	7.7	44.5	3.4	11.1	38.3	21.0	400	1590
V27	0.70	44	24	12	3.7	52	7.1	8.7	0.26	4.8	3.2	41.0	222	52	7.1	47.8	4.63	0.45	7.6	39.0	3.4	11.2	44.2	21.1	436	1590
V28	0.57	49	27	12	3.4	56	5.9	9.5	0.28	2.4	3.5	38.2	238	56	7.0	51.9	4.56	0.44	8.2	43.8	3.8	12.7	60.0	23.7	409	1700
V29	0.43	48	26	12	3.4	53	5.4	9.5	0.27	2.0	3.5	38.6	234	55	6.9	50.4	4.64	0.43	8.1	44.4	3.8	13.3	63.1	23.4	388	1700
V30	0.50	48	26	12	3.3	54	5.7	9.4	0.26	2.3	3.5	38.0	227	54	6.9	49.6	4.67	0.45	8.0	43.6	3.7	13.2	60.4	23.1	385	1720
V32	0.38	47	26	12	3.7	53	5.3	9.4	0.24	2.2	3.4	37.6	230	55	7.2	49.7	4.29	0.40	7.9	39.3	3.7	13.2	62.7	23.0	401	1740
V36	0.42	47	26	12	3.6	52	5.8	9.4	0.26	4.7	3.5	44.9	223	52	7.1	48.2	5.13	0.47	7.8	42.2	3.7	13.5	76.3	23.2	391	1760
V38	0.25	46	26	12	3.1	51	4.5	9.2	0.26	4.2	3.4	37.9	220	52	6.5	48.4	4.89	0.43	7.8	45.2	3.7	13.6	73.4	22.6	325	1680
V39	0.30	46	26	12	3.1	52	5.0	9.2	0.24	2.0	3.4	40.7	222	52	6.3	48.0	4.78	0.44	7.8	43.4	3.7	13.7	73.2	23.0	339	1720
V42	0.56	39	22	10	4.4	43	6.6	7.9	0.23	6.8	3.0	39.4	184	44	7.2	39.9	5.18	0.47	6.5	26.8	3.2	11.8	51.5	20.1	449	1500
V43	0.60	51	27	13	3.8	56	5.9	9.9	0.23	3.5	3.7	33.9	239	56	8.8	52.0	4.16	0.41	8.4	34.2	3.9	12.7	57.2	24.4	446	1640
V44	0.26	48	26	12	3.1	52	6.3	9.4	0.37	2.0	3.5	45.0	227	54	7.2	49.7	5.69	0.57	8.0	51.8	3.7	12.5	63.7	23.7	402	1820
V49	0.21	46	26	11	3.1	50	4.6	9.2	0.29	1.6	3.3	49.2	222	53	6.3	48.4	5.85	0.50	7.6	56.5	3.6	14.1	78.7	22.2	300	1670
V51	0.17	44	25	11	2.9	49	4.3	8.8	0.24	1.3	3.2	45.4	211	50	5.1	46.2	5.00	0.41	7.4	44.5	3.5	13.6	79.0	21.4	279	1530
V52	0.18	47	26	12	2.5	51	4.1	9.1	0.28	1.4	3.3	47.6	222	53	6.0	49.3	5.46	0.46	7.8	38.3	3.6	14.0	81.0	22.2	269	1530
V53	0.32	43	24	11	3.6	47	4.9	8.7	0.27	12.5	3.2	53.8	201	47	6.2	43.8	5.50	0.51	7.1	47.0	3.5	14.5	66.1	21.4	292	1620
V55	0.21	41	23	10	5.0	45	3.9	8.3	0.30	17.5	3.1	54.4	192	46	5.9	42.6	6.27	0.49	6.9	48.8	3.3	13.3	84.6	20.4	281	1530
V58	0.37	47	26	12	4.3	52	4.7	9.4	0.23	3.3	3.5	31.1	223	52	8.0	48.4	4.13	0.35	7.8	34.2	3.7	12.6	60.4	23.6	379	1540
V59	0.79	49	24	14	5.6	56	8.7	9.2	0.37	4.2	3.1	41.7	250	60	11.1	56.6	3.80	0.57	8.5	62.4	3.5	10.3	36.0	21.6	542	2050
V60	0.49	46	25	12	4.5	51	6.8	9.1	0.31	2.7	3.3	39.6	216	51	7.6	48.0	5.06	0.47	7.6	45.8	3.6	12.6	41.3	22.4	419	1740

Table 4
Results of Be-isotope dating. See Table 2 and Fig. 6.

Top	Base	Middle	$^{10}Be/^{9}Be$	2 sigma	Sector	2 sigma	Growth rate
mm	mm	mm	[10^{-7}]	Precision	Age (Ma)	Precision	(mm/Myr)
DV953-R02-S1C							
0	3	1.5	1.02E+00	0.04702	0.40	0.15	
6	9	7.5	3.44E−01	0.01555	2.52	0.15	2.8
12	15	13.5	9.21E−02	0.00425	5.11	0.15	2.3
21	24	22.5	1.01E−02	0.00056	9.45	0.16	2.1
30	33	31.5	2.17E−03	0.00022	12.46	0.23	3.0
DV954-R10-S2A							
0	3	1.5	1.21E+00	0.05815	0.06	0.11	
6	9	7.5	5.34E−01	0.02471	1.66	0.11	3.8
12	15	13.5	1.90E−01	0.00870	3.69	0.11	3.0
21	24	22.5	3.54E−02	0.00171	6.99	0.11	2.7
DV956-R15-S1D							
0	3	1.5	1.11E+00	0.05226	0.23	0.10	
9	12	10.5	2.74E−01	0.01260	2.97	0.10	3.3
18	21	19.5	8.10E−02	0.00392	5.36	0.10	3.8
27	30	28.5	1.91E−02	0.00101	8.19	0.11	3.2
36	39	37.5	7.35E−03	0.00053	10.07	0.15	4.8
45	48	46.5	2.83E−03	0.00024	11.94	0.17	4.8
57	60	58.5	3.52E−04	0.00020	16.03	1.12	2.9
DV958-R12-S2D							
0	3	1.5	8.66E−01	0.04016	0.71	0.10	
15	18	16.5	4.70E−02	0.00230	6.43	0.11	2.6
30	33	31.5	6.86E−03	0.00043	10.20	0.13	4.0
52	56	54	5.52E−05	0.00023	19.67	8.31	2.4
DV959-R11-S1							
0	3	1.5	9.93E−01	0.04750	0.44	0.10	
12	15	13.5	1.42E−01	0.00729	4.26	0.11	3.1
24	27	25.5	1.85E−02	0.00112	8.26	0.13	3.0

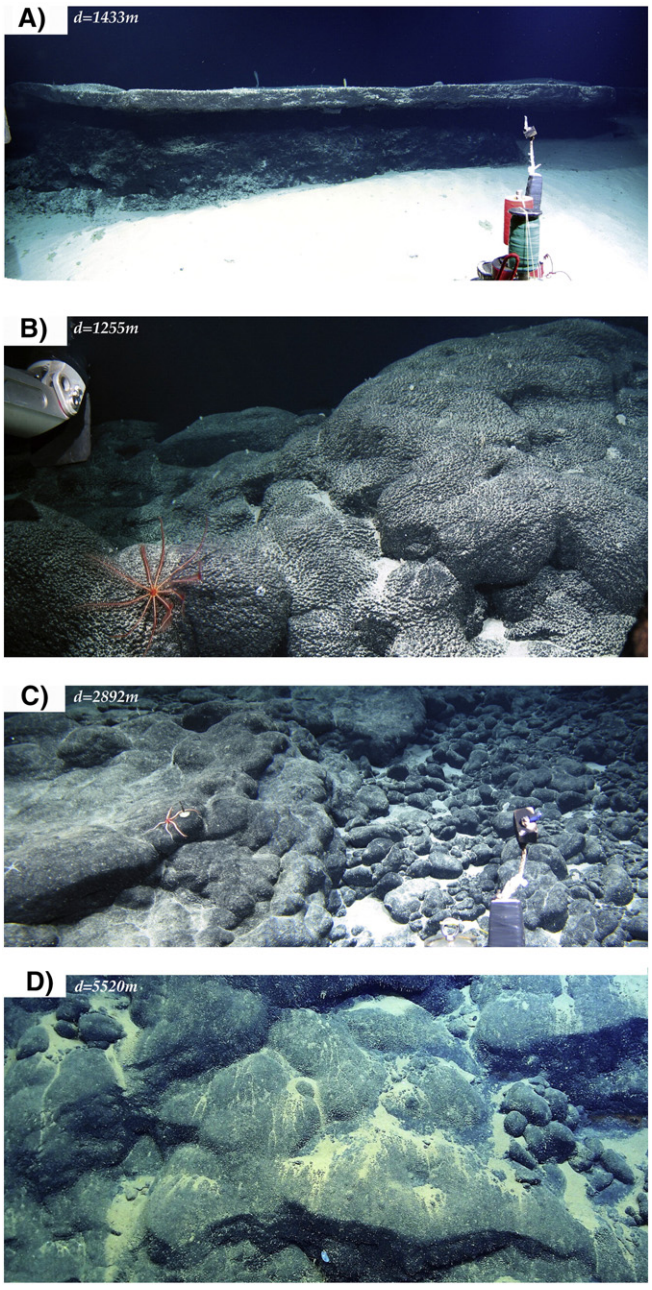

Fig. 4. Photos of ferromanganese crusts on the seafloor. A) Near the top of seamount, 8-cm-thick crust covers a Rudist reef, substrate partly eroded, B) knobby surface of the ferromanganese crusts near the summit margin, substrate is calcareous conglomerate, C) middle of the slope and boulders coated with crusts, D) knobby surface of 2–6 cm thick crusts at the deepest part of steep outcrop of consolidated slump deposit. Width of each frame is about 4 m.

seamount (Fig. 9) are similar to each other. However, when compared to a crust from off the Hawaiian Islands (Vonderhaar et al., 2000), the secular trend is quite different. This implies that both regional and local paleogeological and oceanographic environments influence the temporal chemical and mineralogical variations within the crusts.

Among the patterns of elemental distribution reported (e.g., Xiangwen et al., 2007; Wen et al., 1997) for crusts, the most dramatic change in chemical composition is the dual structure (older and younger generations) divided by a marked change in physical and mineralogical properties. The dominant dual structure (showing a younger earthy black, apatite-free, friable generation, and an older apatite-rich, hard, phosphatized generation), first described by Halbach et al. (1989), was observed in all crusts of this study thicker than about 5 cm. This microstratigraphic correlation in structure suggests a regional or global change in the oceanographic environment, such as changes in ocean circulation (Nishi et al., 2017).

5.3. Age and rate of growth

The ages and growth rates have been measured mainly by $^{10}Be/^{9}Be$ ratios, supported by paleomagnetic stratigraphy, and other radiochemical and paleontological methods (Mangini et al., 1990; Hein et al., 1993; Nielsen et al., 2007; Oda et al., 2011; Noguchi et al. 2017). We tried several different radiometric dating methods for the northwest Pacific Fe-Mn crusts for cross-checking using Os-Re (Tokumaru et al., 2015) and U series (Goto et al., 2014; Yamaoka et al., 2017-in this volume) as well. The range of Be dating goes back to about 12 Ma by direct measurement, but related available age models have been extrapolated back to 17 Ma (Nishi et al., 2017). Nishi et al. (2017) determined that growth rates for Takuyo-Daigo crusts were fairly constant (2.1–3.2 mm/Ma) and the age of the surface of each crust indicates modern precipitates. In general, constant rates of growth and fairly constant mass accumulation of manganese and major elements are indicated for regional areas and a wide range of water depths (Fig. 8, Table 4). The growth of the younger generation started at ~17 Ma ago or later. The rates are remarkably constant within and below the OMZ, indicating that the hydrogenetic precipitation took place at all depths in the seawater column. The curves for four samples from the slope show a pattern typical of crusts from seamounts in the northwestern Pacific Basin (Usui et al., 2007; see in Fig. 8).

Based on metal fluxes (or mass accumulation rate) for Fe-Mn crusts (Sato and Usui, unpublished, 2009), calculated as MF for major elements

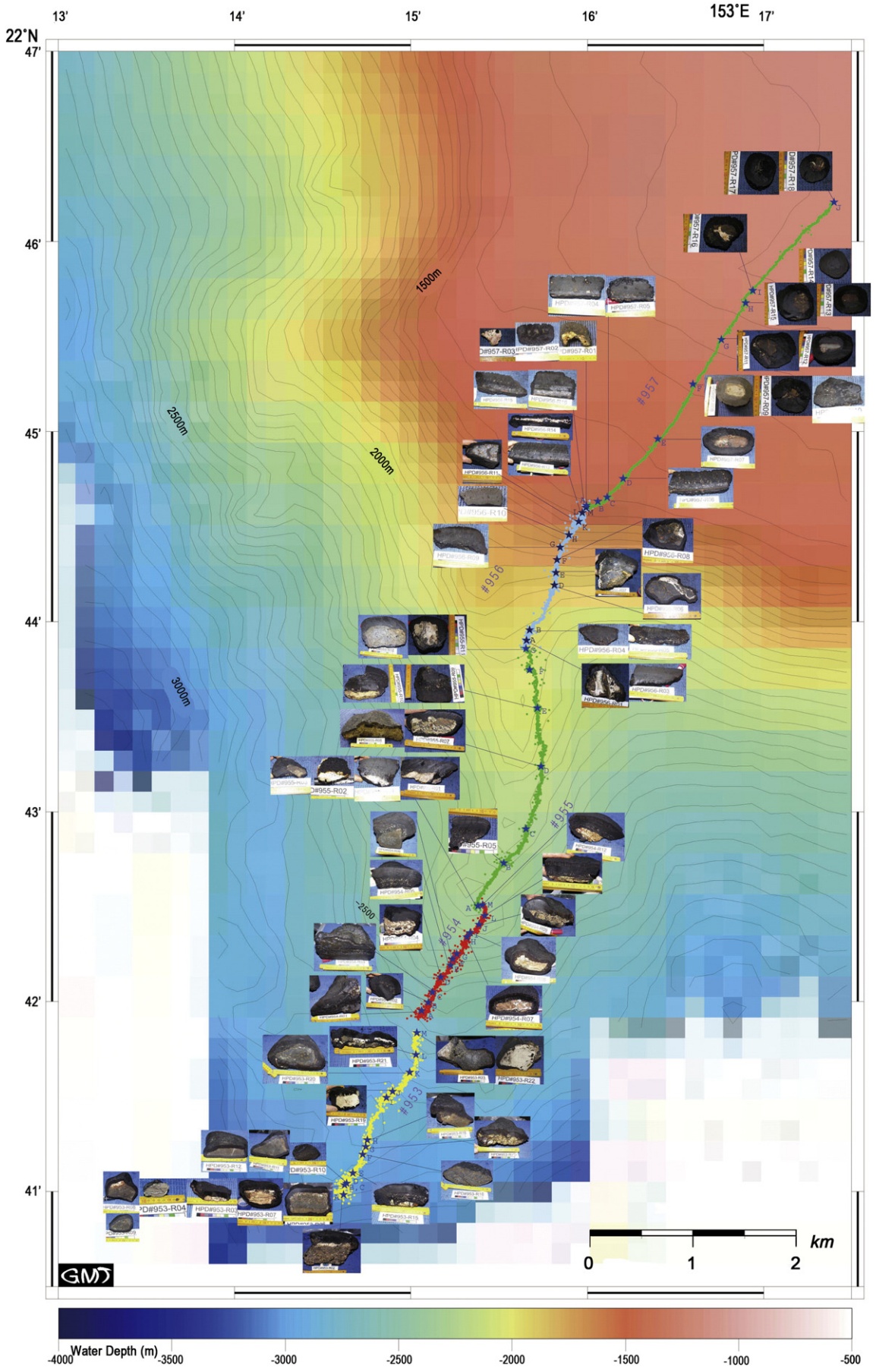

Fig. 5. Survey track lines, sample location, and section of samples at the southern end of the seamount, at 3000 to 1200 m water depths. All outcrops are covered with crusts.

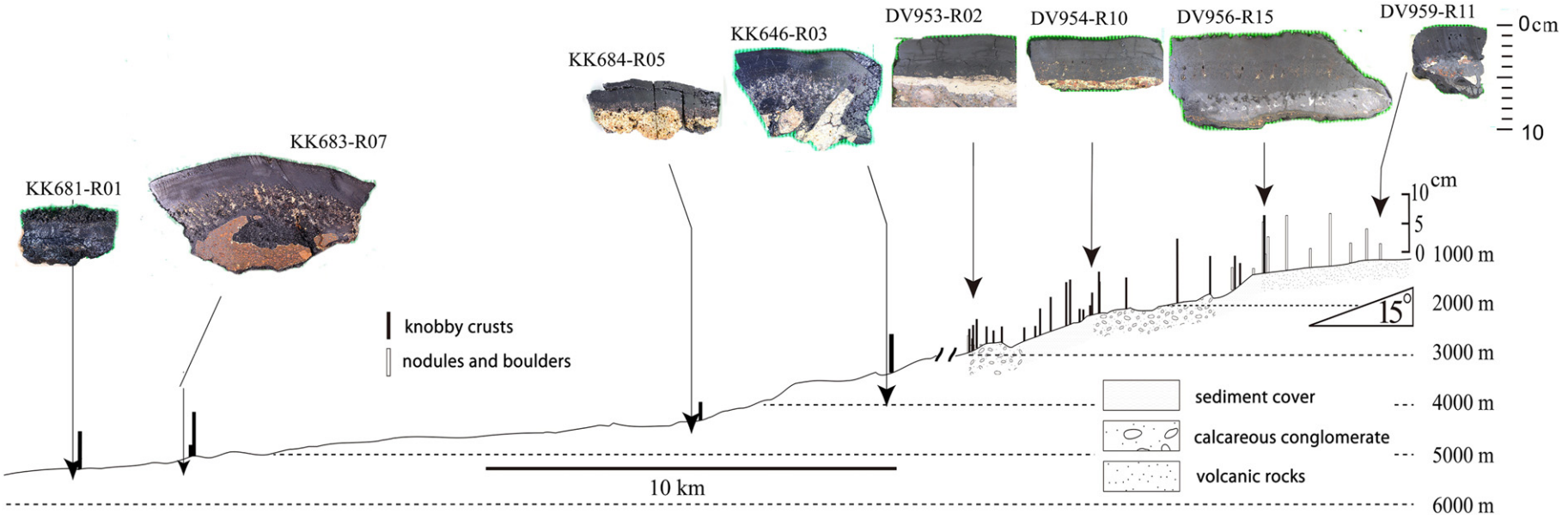

Fig. 6. Topography of the southernmost ridge and occurrence of crusts. Bars show maximum thickness of crusts at each site. No vertical exaggeration. See thick crusts up to 10 cm thick commonly over the volcanic rock substrate.

Fe and Mn, are in the range of 0.07–0.11 g/cm^2/Myr with very small fluctuations with water depth between 1000 and 3000 m (Fig. 10). The figure also shows constant nature of secular variations. On the other hand, the most remarkable trend is that of cobalt, showing an increase at shallower depth between 1000 and 3000 m by a factor of 2 or more

5.4. Water depth control of the modern precipitates

Crusts have grown in layers over millions of years and have variable morphologies and growth surfaces (Fig. 7). The chemistry and mineralogy are mostly determined by the oceanographic and geological conditions (Glasby et al., 2010). We examined variations in the composition of surface scrapes with water depth. Our CTD-DO sensor on the ROV measured a clear minimum of DO at 900 to 1000 m water depths during every cruise conducted during 2009–2013. Remarkably, the DO profile measured during each dive (#953–#957) at the seabed during surveying and uplift to the mother ship are exactly the same (~0.5 mL/L), suggesting that the OMZ directly intersects rock outcrops on the upper part of the seamount.

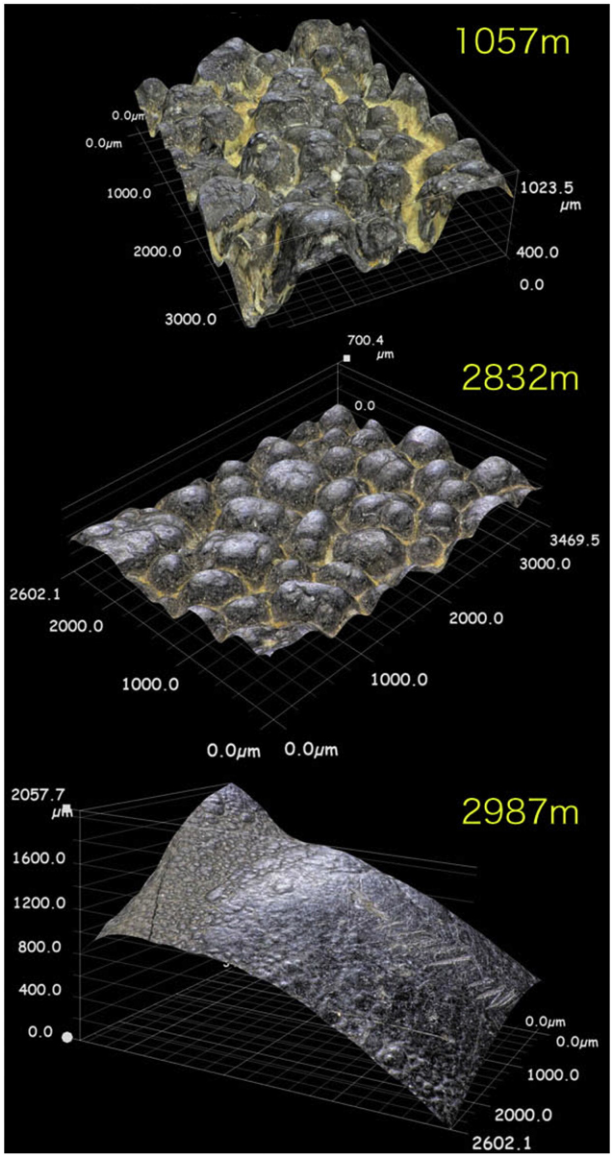

Fig. 7. Digital micrographs of surface texture of crusts from different water depths. The botryoids are more rugged (sub-millimeter scale) at shallower water depths suggesting abundant supply of biogenic and detrital materials.

The trend of water-depth and chemical composition of surface scrapes (uppermost ≤ 1 mm) indicates clear correlations with Fe, Mn and Co (Fig. 11) and Fe/Mn (Fig. 12), while other elements show no significant change or a similar trend as Fe/Mn except for Ti. Cobalt is the most abundant redox-controlled element after Mn in the crusts, and has the highest negative correlation coefficients with water depth and dissolved oxygen (Figs. 11 and 12).

5.5. Conditions of formation

Our data indicate that both Fe oxyhydroxide and Mn oxide have been accumulating continuously as crusts at similar rates of growth and similar metal fluxes throughout the sampled water depths, even within the OMZ. Precipitation has been taking place continuously for at least 17 Ma or longer. These data suggest a generally rather uniform environment for deposition of these hydrogenetic crusts.

Another factor that controls the abundance of crusts may be geological stability of the substrate rock and the sedimentary history over the seamount. Mass wasting or rapid sedimentation may interrupt or reset continuous deposition, which may have been completed at the early stage of seamount evolution. Thus, variable thicknesses of crusts mainly depend simply on the time of exposure to seawater, if not otherwise disrupted. The evolution of seamounts and the Fe-Mn crusts is summarized as: 1) volcanic eruption, wave-cut erosion on the edifices that became islands, 2) reef building, subsidence, and 3) continuous deposition of most of the Fe-Mn crusts in pelagic environments.

It has been well hypothesized that the concentration of dissolved Mn^{2+} increases in the OMZ and is therefore a major source of Mn for producing thick hydrogenetic crusts nearby outside the OMZ (e.g., Koschinsky and Halbach, 1995). Earlier study on seawater chemistry (e.g., Bruland et al., 1994) suggested that most common dissolved complex of Mn is in a reduced divalent state in oxygen depleted seawater. However, our finding of abundant growth of crusts within and below the OMZ and clear oxygen depletion over the slope of a seamount is not well supported with this model even though dissolved Mn^{2+} increases in the OMZ. Our results favor a model where most of Mn can be stable as oxidized colloids in the OMZ since oxidation of Mn is completed in the OMZ. Molecular characterization of microbial ecosystem

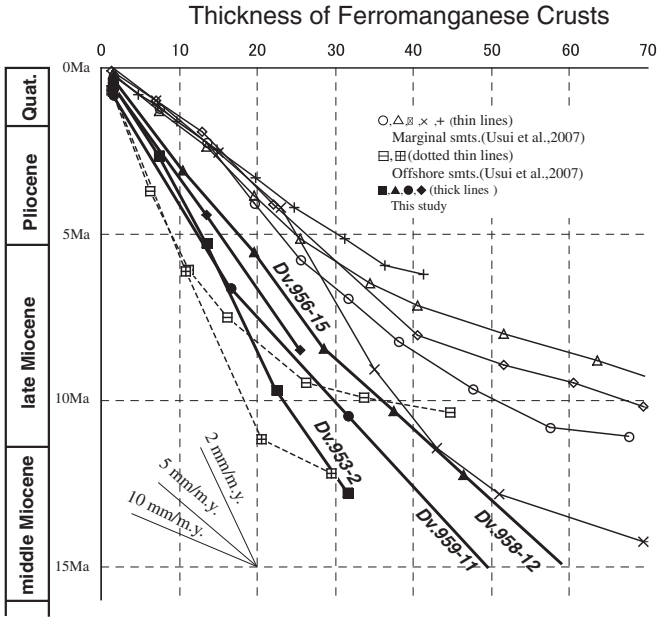

Fig. 8. Growth curves for the ferromanganese crust samples from the Takuyo-Daigo seamount (thick lines). Thin solid lines and thin broken lines are crusts from marginal seamounts and offshore seamounts (Usui et al., 2007) for comparison.

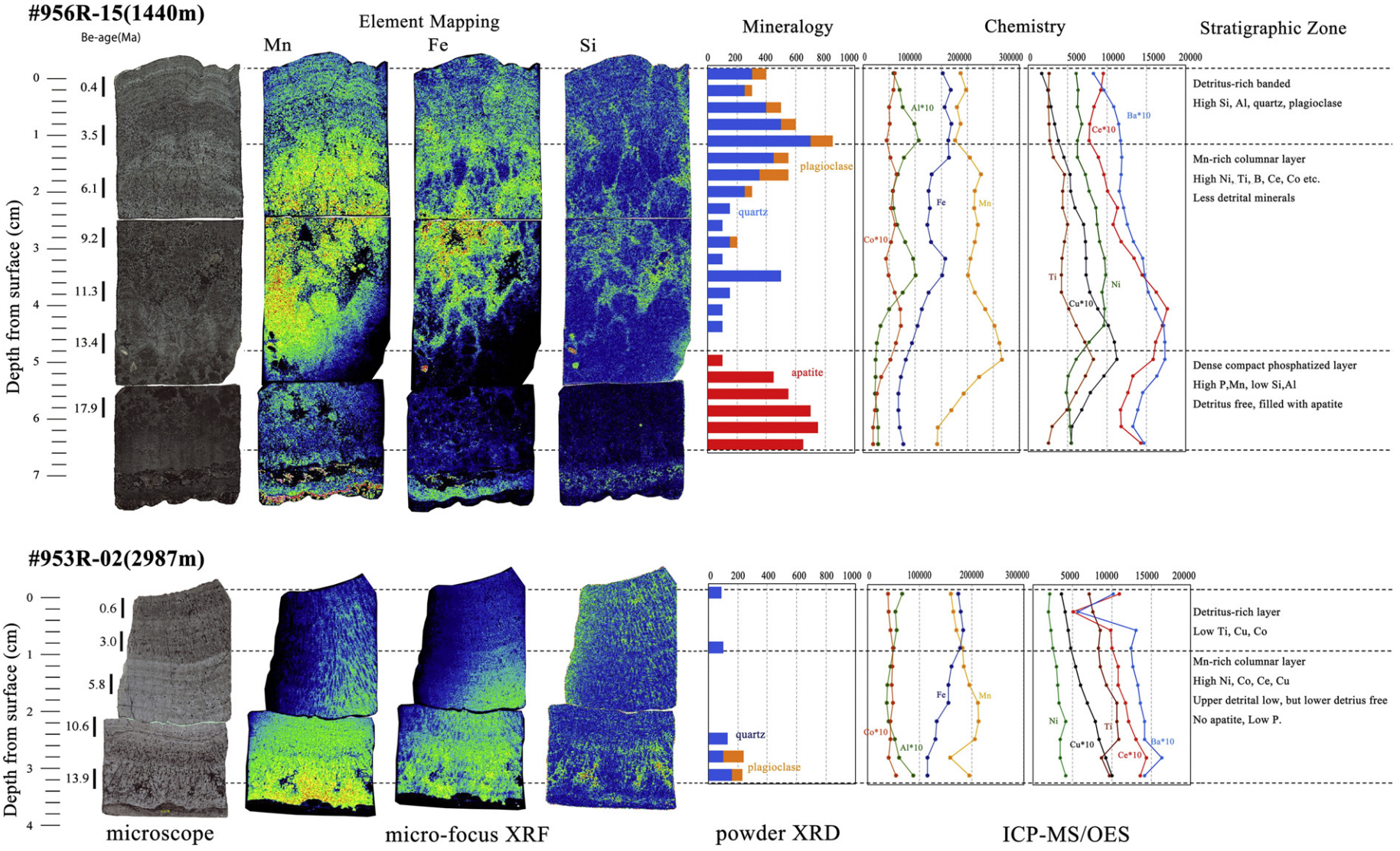

Fig. 9. Secular profiles of chemical and mineral composition in the sections of crusts. General trend of metallic elements is similar among crusts from different water depths. Note the deeper crust is missing the P-rich old generation.

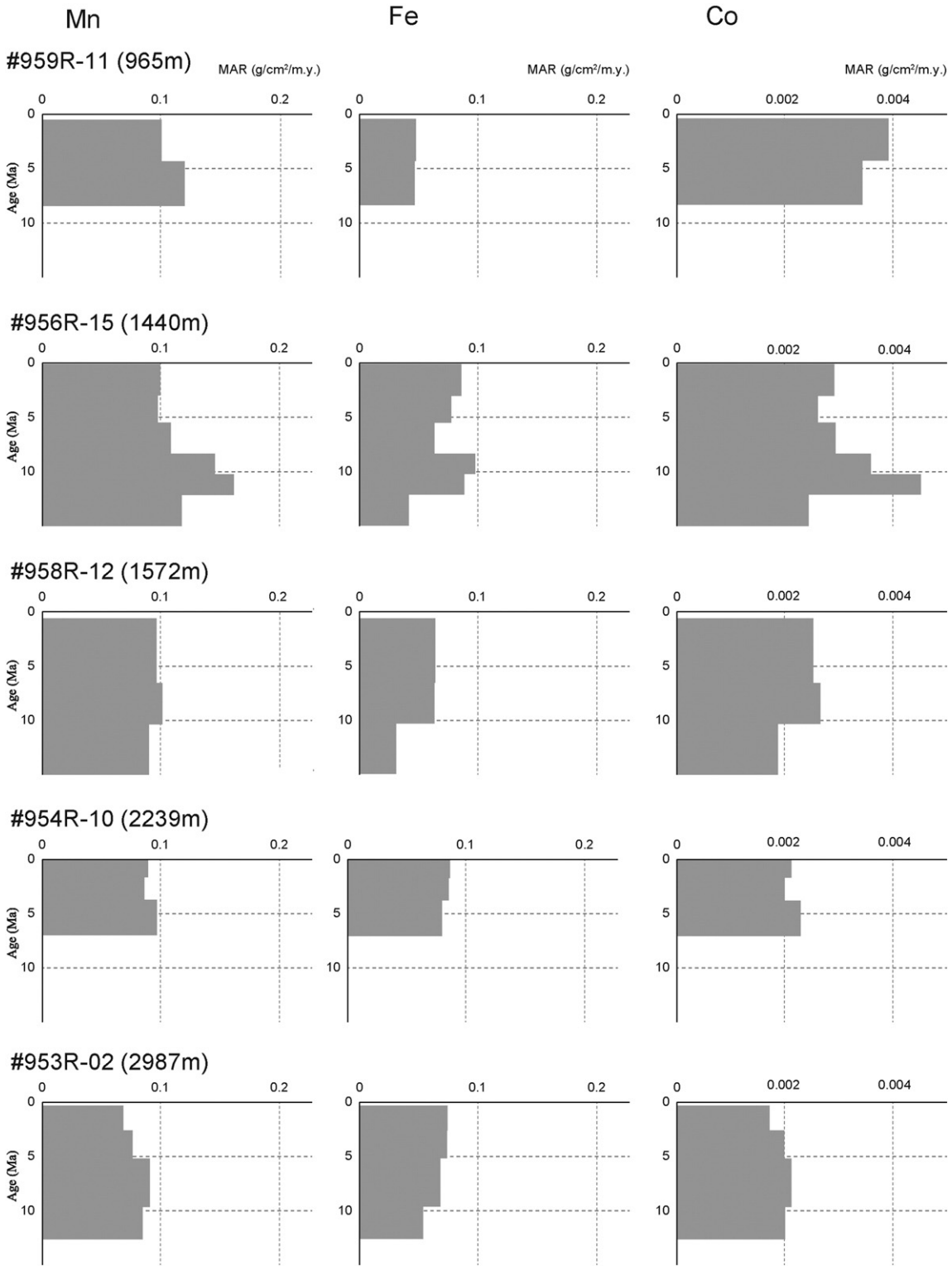

Fig. 10. Metal flux for Mn, Fe, and Co of five crusts at different water depths. Each graph show Flux vs age. Major components, Mn and Fe, show no clear trend, but Co flux clearly decreases in deeper water.

on the surfaces of crusts on the seamount (Nitahara et al., 2011) indicated prevailing ammonia-oxidizing chemolithoautotrophs but no significant difference of microbial community in the OMZ. The state of Mn in seawater and precipitates for crusts should be investigated in more detail with on-site measurement and observation of Fe-Mn crusts as well as their environs. Understanding of dissolved/particulate forms of the metals, and physicochemical and microbiological environments (Halbach et al., 1983; Bruland et al., 1994) are required to conclude the questions.

It is reasonable to assume that the concentrations of minor metals as well as the precipitation of Mn and Fe are controlled by seawater chemistry, physicochemical (e.g., Takahashi et al., 2000; Chester, 2003; Hein

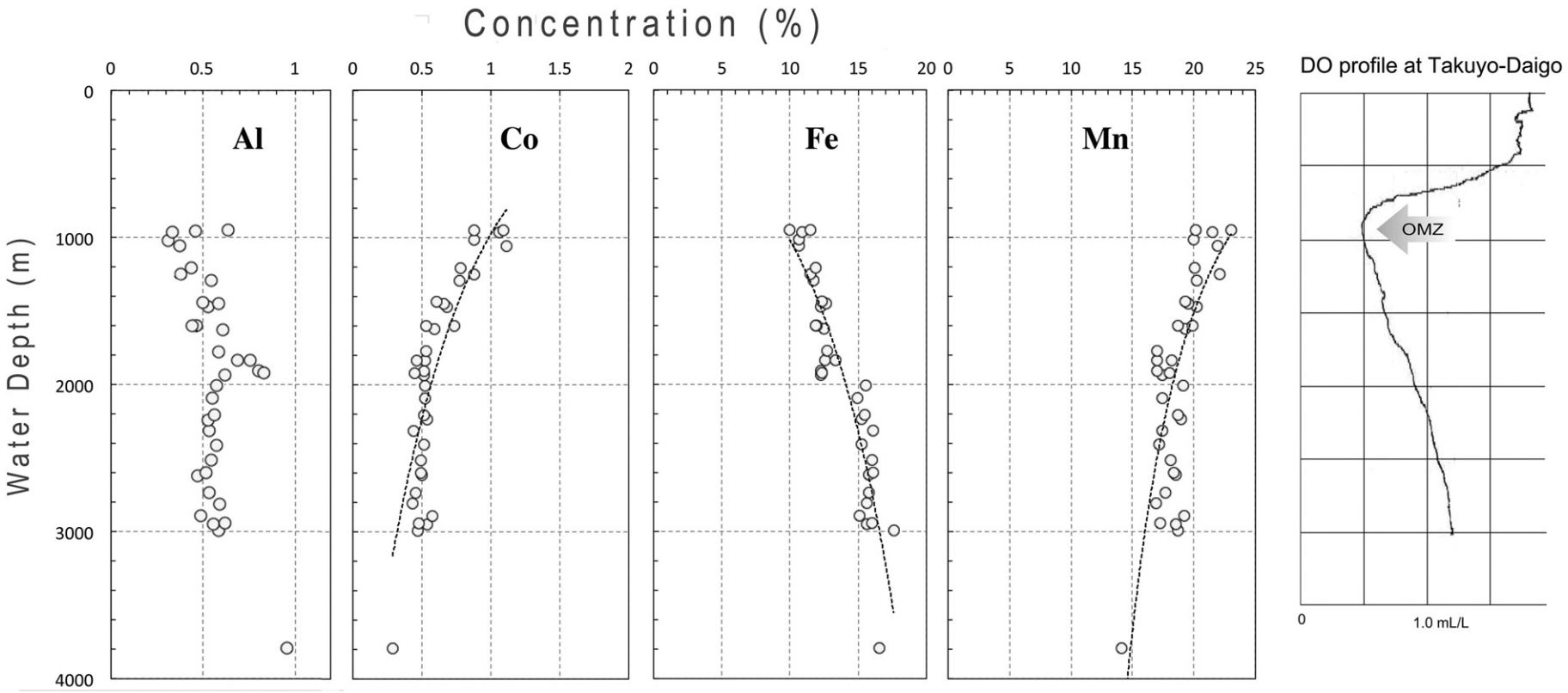

Fig. 11. Chemical composition of scrapes from very surface of crusts vs water depth. Co and Mn/Fe decrease with depth, while Al shows no change.

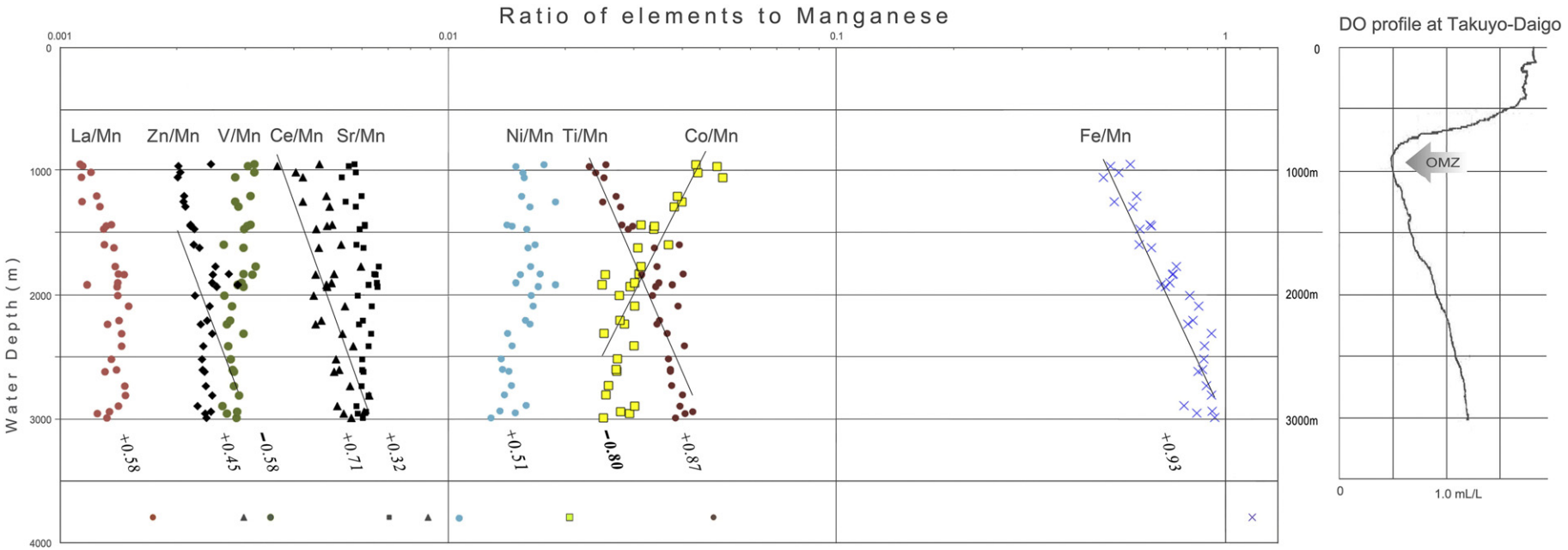

Fig. 12. Metal concentration ratioed to Mn concentration for surface scrapes of crusts vs water depth, demonstrating selective sorption of the elements to hydrogenetic vernadite. Co has the highest correlation coefficients with water depth. Note a strong negative correlation of Co/Mn, and a positive correlation of Ti/Mn with water depth.

et al., 2000) and sedimentary (e.g., Aplin and Cronan, 1985) conditions, and reactivity of Fe and Mn oxides with dissolved compounds. According to the Koschinsky and Halbach's (1995) colloidal-chemical model of metal accumulation, Mn and Fe oxide nano-particles are strongly charged and thus highly reactive with selected dissolved ions in seawater, which controls the chemical variability of Fe-Mn crusts. They showed that Mn oxide is negatively charged in seawater and attracts Ni, Co, Cu, Zn, Cd, Pb, Tl and light REE cations, while iron oxide is positively charged and attracts As, Mo, V, Ti, P, Zr and heavy REE anions. We compared the metals that are mostly incorporated in the Fe-bearing vernadite with water depth, and whether the concentration to Mn or Fe in vernadite is constant or variable.

The result (Fig. 12) showed a strong depth dependency of only Co (negative correlation: −0.80) and Ti (positive correlation: +0.87) among other metals. The depth dependency of Ti is explained by their model as Ti hydroxide is exclusively adsorbed to iron oxide, but the strong dependency for Co is probably related to the high concentration of Co^{2+} in OMZ (Nozaki, 2001) and structural effect of phyllomanganate mineral below the OMZ, as well as electrochemical sorption. Co content and Co/Mn ratio vary by a factor of >2.0 between depths 800 m and 3000 m on the seamount, which is somewhat greater than some regional variations of the element, again supporting that seawater conditions are important controlling parameters of the precipitates. The monoclinal water-depth dependency of Co in the modern surface precipitates is clear, rather suggesting its strong redox-sensitive nature of cobalt in seawater. Manceau et al. (1997) suggested the effective concentration of Co onto Mn-oxide surface based on molecular-scale structural analysis of manganese minerals. Takahashi et al. (2007) pointed out that dissolved Co^{2+} in sea water is easily exchanged with divalent or trivalent Mn and readily oxidized and fixed as Co^{3+} in the phyllomanganate structure. We consider that the dependency is related to an elevated concentration of Co in the OMZ as well as specific adsorptive nature of the manganese minerals. Similar structural control is proposed for Ce, Pb, W, and Te by means of laboratory experiments and speciation with XANES (Takahashi et al., 2000; Kashiwabara et al., 2011, 2013, 2014).

Future research should include global- to nano-scale characterization of marine Fe-Mn deposits to develop robust models for the selective concentration of metals. Our approach is for additional studies of molecular-scale analysis, laboratory experiments, in situ experiments, microbial analysis, high-resolution chemical and structural analyses, and further fine-scale dating (e.g., Kashiwabara et al., 2013; Nitahara et al., 2011; Morishita and Usui, 2015). Many more on-site exploration and geological surveys using ROV, AUV, and submersibles, as well as laboratory analyses, are needed and planned.

6. Summary

ROV observations and sampling along the slope of the large flat-topped Takuyo-Daigo seamount have provided us with detailed geological characteristics of hydrogenetic Fe-Mn crust deposits and their variability in abundance and composition. Our geological growth model is based on high-resolution Be-isotope dating supported by paleomagnetic and paleontological data.

Major conclusions are as follows:

1) Hydrogenetic precipitation of Fe and Mn took place continuously at rates of 2–3 mm/Myr for at least the past 17 Myr, producing up to 105-mm-thick crust deposits at a wide-range of water depths (800–5500 m) including within the OMZ.

2) Regional variation in abundance (thickness) is basically controlled by evolution of the seamount, nature of substrate rock, and sedimentary history. The flux of Fe and Mn to the crusts has not changed much during their growth over millions of years in a wide range of water depth.

3) Composition of modern precipitates (surface scrapes of crusts) varies with water depth. Especially Co concentration is strongly dependent on water depth and mirrors the profile of Mn, showing a strong increase in Co with decreasing water depth. These distributions are probably controlled by the redox state of seawater, effective incorporation into Mn minerals from 800 to 5500 m, and dilution by Fe and other phases.

Acknowledgements

We deeply express our thanks to the following organizations: Kochi University, Geological Survey of Japan (GSJ/AIST), Japan Agency for Marine and Earth Sciences and Technology (JAMSTEC), and Japan Oil, Gas, and Metal Exploration Corporation (JOGMEC); and to all staff from those organizations for their continuous support and collaboration during cruises and laboratory analyses. Fruitful discussions and suggestions from reviewers J. R. Hein and J. Gonzalez, colleagues, J-K Kang, S.W. Chang and C. Morgan are deeply acknowledged. Supporting technical staff and crew members of cruises are appreciated, as our research would not have been possible without their efforts and cooperation.

References

Aplin, A.C., Cronan, D.A., 1985. Ferromanganese oxide deposits from the Central Pacific Ocean, I. Encrustations from the Line Islands Archipelago. Geochim. Cosmochim. Acta 49, 427–436.
Bayon, G., German, C.R., Burton, K.W., Nesbitt, R.W., Rogers, N., 2004. Sedimentary Fe–Mn oxyhydroxides as paleoceanographic archives and the role of aeolian flux in regulating oceanic dissolved REE. Earth Planet. Sci. Lett. 224, 477–492.
Bruland, K.W., Orians, K.J., Cowen, J.P., 1994. Reactive trace metals in the stratified central North Pacific. Geochim. Cosmochim. Acta 58 (15), 3171–3182.
Chester, R., 2003. Marine Geochemistry. Second edition. Blackwell Publ. Co., p. 506.
Davis, G.F., Pribac, F., 1997. Mesozoic seafloor subsidence and the Darwin Rise, past and present. In: Pringle, M.S., et al. (Eds.), The Mesozoic Pacific: Geology, Tectonics, and Volcanism. AGU Geophys. Monogr 77, pp. 39–52.
Glasby, G.P., 2000. Manganese: predominant role of nodules and crusts. Marine Geochemistry. Springer, pp. 335–372.
Glasby, G.P., Ren, X., Shi, X., Pulyaeva, I.A., 2007. Co-rich Mn crusts from Magellan seamount cluster: the long journey through time. Geo-Mar. Lett. 27, 315–323.
Glasby, G.P., Mountain, B., Vineesh, T.C., Banakar, V., Rajani, R., Ren, X., 2010. Role of hydrology in the formation of Co-rich Mn crusts from the equatorial N Pacific, Equatorial S Indian Ocean and the NE Atlantic Ocean. Resour. Geol. 60, 165–177.
Goto, K.T., Anbar, A.D., Gordon, G.W., Romaniello, S., Shimoda, G., Takaya, Y., Tokumaru, A., Nozaki, T., Suzuki, K., Machida, S., Hanyu, T., Usui, A., 2014. Uranium isotope systematics of ferromanganese crusts in the Pacific Ocean: implications for the marine $^{238}U/^{235}U$ isotope system. Geochim. Cosmochim. Acta 146, 43–58.
Graham, I., Ditchburn, R.G., Zondervan, A., 2004. Chronostratigraphy of ODP 181, Site 1121 sediment core (Southwest Pacific Ocean) using $^{10}Be/^{9}Be$ dating of entrapped ferromanganese nodules. Mar. Geol. 205 (1–4), 227–247.
Halbach, P., Puteanus, D., 1984. The influence of the carbonate dissolution rate on the growth and composition of Co-rich ferromanganese crusts from Central Pacific seamount areas. Earth Planet. Sci. Lett. 68 (1), 73–87.
Halbach, P.E., Segl, M., Puteanus, D., Mangini, A., 1983. Co-flux and growth rates in ferromanganese deposits from Central Pacific seamount areas. Nature 5928, 716–719.
Halbach, P.E., Sattler, C.-D., Teichmann, F., Wahsner, M., 1989. Cobalt-rich and platinum-bearing manganese crust deposits on seamounts: nature, formation, and metal potential. Mar. Min. 8, 23–39.
Halliday, A.N., Lee, D.-C., Christensen, J.N., Rehkamper, M., Yi, W., Luo, X., Hall, C.M., Ballentine, C.J., Pettke, T., Stirling, C., 1998. Applications of multiple collector-ICPMS to cosmochemistry, geochemistry, and paleoceanography. Geochim. Cosmochim. Acta 62 (6), 919–940.
Hein, J.R., Yeh, H.-W., Gunn, S.H., Sliter, W.V., Benninger, L.M., Wang, C.-H., 1993. Two major episodes of Cenozoic phosphogenesis recorded in equatorial Pacific seamount deposits. Paleoceanography 8, 293–311.
Hein, J.R., Koschinsky, A., Bau, M., Manheim, F.T., Kang, J.-K., Roberts, L., 2000. Cobalt-rich ferromanganese crusts in the Pacific. In: Cronan, D.S. (Ed.), Handbook of Marine Mineral Deposits. CRC Press, Boca Raton, pp. 239–279.
Hein, J.R., Conrad, T.A., Frank, M., Christl, M., Sager, W.W., 2012. Copper-nickel-rich, amalgamated ferromanganese crust-nodule deposits from Shatsky Rise, NW Pacific. Geochem. Geophys. Geosyst. 13, Q10022.
Hein, J.R., Mizell, K., Kochinsky, A., Conrad, T.A., 2013. Deep-ocean mineral deposits as a source of critical metals for high-and green-technology applications: comparison with land-based resources. Ore Geol. Rev. 51, 1–15.
Jeong, K.S., Jung, H.S., Kang, J.K., Morgan, C.L., Hein, J.R., 2000. Formation of ferromanganese crusts on northwest intertropical Pacific seamounts: electron photomicrography and microprobe chemistry. Mar. Geol. 162, 541–559.
Kashiwabara, T., Takahashi, Y., Tanimizu, M., Usui, A., 2011. Molecular-scale mechanisms of distribution and isotopic fractionation of molybdenum between seawater and ferromanganese oxides. Geochim. Cosmochim. Acta 75, 5762–5784.

Kashiwabara, T., Takahashi, Y., Marcus, M.A., Uruga, T., Tanida, H., Terada, Y., Usui, A., 2013. Tungsten species in natural ferromanganese oxides related to its different behavior from molybdenum in oxic ocean. Geochim. Cosmochim. Acta 106, 364–378.
Kashiwabara, T., Oishi, Y., Sakaguchi, A., Sugiyama, T., Usui, A., Takahashi, Y., 2014. Chemical processes for the extreme enrichment of tellurium into marine ferromanganese oxides. Geochim. Cosmochim. Acta 131, 150–163.
Koppers, A.A.P., Staudigel, H., Wijbrans, J.R., 1998. The Magellan seamount trail: implications for Cretaceous hotspot volcanism and absolute Pacific plate motion. Earth Planet. Sci. Lett. 163, 53–68.
Koppers, A.A.P., Staudigel, H., Pringle, M.S., Wijbrans, J.R., 2003. Short-lived and discontinuous intraplate volcanism in the South Pacific: hot spots or extensional volcanism? Geochem. Geophys. Geosyst. 4 (10), 1–49 (AGU and the Geochemical Society).
Korschinek, G., Bergmaier, A., Faestermann, T., Gerstmann, U.C., Knie, K., et al., 2010. A new value for the half-life of ^{10}Be by heavy-ion elastic recoil detection and liquid scintillation counting. Beam Interactions Mater Atom 268 (2), 187–191.
Koschinsky, A., Halbach, P., 1995. Sequential leaching of marine ferromanganese precipitates: genetic implications. Geochim. Cosmochim. Acta 59 (29), 5113–5132.
Koschinsky, A., Halbach, P., Hein, P., Mangini, A., 1996. Ferromanganese crusts as indicators for paleoceanographic events in the NE Atlantic. Geol. Rundsch. 85 (3), 567–576.
Larson, K.M., Freymueller, J., 1995. Relative motions of the Australian, Pacific and Antarctic Plates estimated by the Global Positioning System. Geophys. Res. Lett. 22, 37–40.
Manceau, A., Drits, V.A., Silvester, E., Bartoli, C., Lanson, B., 1997. Structural mechanism of Co^{2+} oxidation by the phyllomanganate buserite. Am. Mineral. 82 (11–12), 1150–1175.
Mangini, A., Eisenhauer, A., Walter, P., 1990. Response of manganese in the ocean to the climatic cycles in the. Quaternary Paleoproductivity and Paleochemistry of the Oceans 5 (5), 811–821.
Manheim, F.T., Lane-Bostwick, C.M., 1988. Cobalt in ferromanganese crusts as a monitor of hydrothermal discharge on the Pacific sea floor. Nature 335 (1), 89–92.
Morishita, Y., Usui, A., 2015. Microanalysis of platinum in hydrogenetic ferromanganese crust using SIMS. Geochem. J. 49 (6), e21–e26.
Nakanishi, M., Winterer, E.L., 1998. Tectonic history of the Pacific-Farallon-Phoenix triple junction from Late Jurassic to Early Cretaceous: an abandoned Mesozoic spreading system in the Central Pacific Basin. J. Geophys. Res. 103, 12453–12468.
Nakanishi, M., Sagar, W.W., Klaus, A., 1999. Magnetic lineations within Shatsky Rise, Northwest Pacific ocean: Implications for hot spot-triple junction interaction and oceanic plateau formation. J. Geophys. Res. B: Solid Earth 104 (B4), 7539–7556.
Nielsen, S.G., Mar-Gerrison, S., Gannoun, A., LeRowe, D., Klemm, V., Halliday, A.N., Burton, K.W., Hein, J.R., 2007. Thallium isotope for a permanent increase in marine organic carbon export in the early Eocene. Earth Planet. Sci. Lett. 278, 297–307.
Nishi, K., Usui, A., Nakasato, Y., Yasuda, H., 2017. Formation age of the dual structure and environmental change recorded in hydrogenetic ferromanganese crusts from Northwest and Central Pacific seamounts. Ore Geol. Rev. 87, 62–70.
Nitahara, S., Kato, S., Urabe, T., Usui, A., Yamagishi, A., 2011. Molecular characterization of the microbial community in hydrogenetic ferromanganese crusts of the Takuyo-Daigo Seamount. FEMS Microbiol. Lett. 321 (2), 121–129.
Noguchi, A., Yamamoto, Y., Nishi, K., Usui, A., Oda, H., 2017. Paleomagnetic study of ferromanganese crusts recovered from the northwest Pacific – testing the applicability of the magnetostratigraphic method to estimate growth rate. Ore Geol. Rev. 87, 16–24.
Nozaki, Y., 2001. Elemental distribution: Overview. In: Steele, J.H., Thorpe, S.A., Turekian, K.K. (Eds.), Encyclopedia of Ocean Sciences Vol. 2. Academic Press, London, pp. 840–845.
Oda, H., Usui, A., Miyagi, I., Joshima, M., Weiss, B.P., Shantz, C., Fong, L.E., Baudenbacher, F.J., 2011. Ultrafine-scale magnetostratigraphy of marine ferromanganese crust. Geology 39 (3), 227–230.
Okamoto, N., Usui, A., 2014. Geophysical and geological exploration of cobalt-rich ferromanganese crusts: an attempt of small-scale mapping on a micronesian seamount. Mar. Georesour. Geotechnol. 28 (3), 192–206.
Puteanus, D., Halbach, P., 1988. Correlation of Co concentration and growth rate - a method for age determination of ferromanganese crusts. Chem. Geol. 69, 73–85.
Schlacher, T.A., Baco, A.R., Rowden, A.A., O'hara, T.D., Clark, M., Kelley, C., Dower, J.F., 2014. Seamount benthos in a cobalt rich crust region of the Central Pacific: conservation challenges for future seabed mining. Divers. Distrib. 20, 491–502.
Suave, R.E., Pichocki, C., Pautot, G., Hoffert, M., Morel, Y., Voisset, M., Monti, S., Amosse, J., Kosakevitch, A., 1989. Geological and mineralogical study of Co-rich ferromanganese crusts from a submerged atoll in the Tuamotu Archipelago (French Polynesia). Mar. Geol. 87, 227–247.
Takahashi, Y., Shimizu, H., Usui, A., Kagi, H., Nomura, M., 2000. Direct observation of tetravalent cerium in ferromanganese nodules and crusts by X-ray-absorption near-edge structure (XANES). Geochim. Cosmochim. Acta 64, 2929–2935.
Takahashi, Y., Manceau, A., Geoffroy, N., Marcus, M.A., Usui, A., 2007. Chemical and structural control of the partitioning of Co, Ce, and Pb in marine ferromanganese oxides. Geochim. Cosmochim. Acta 71, 984–1008.
Templeton, A.S., Knowles, E.J., Eldridge, D.L., Arey, B.W., Dohnalkova, A.C., Webb, S.M., Bailey, B.E., Tebo, B.M., Staudigel, H., 2009. A seafloor microbial biome hosted within incipient ferromanganese crusts. Nat. Geosci. 2, 872–876.
Thornton, B., Asada, A., Bodenmann, A., Sangekar, M., Ura, T., 2013. Instruments and methods for acoustic and visual survey of manganese crusts. IEEE J. Ocean. Eng. 38, 186–203.
Tokumaru, A., Nozaki, T., Suzuki, K., Goto, K., Chang, Q., Kimura, J., Tkaya, Y., Kato, Y., Usui, A., Urabe, T., 2015. Re–Os isotope geochemistry in the surface layers of ferromanganese crusts from the Takuyo Daigo Seamount, northwestern Pacific Ocean. Geochem. J. 49 (3), 233–241.
Usui, A., 2010. Marine Minerals-Future Resources for Rare Metals. Ohmsha Co. Ltd. ISBN978-4-274-50287-3, p. 198 (in Japanese).
Usui, A., Okamoto, N., 2010. Geophysical and geological exploration of cobalt-rich ferromanganese crusts: an attempt of small-scale mapping on a Micronesian seamount. Mar. Georesour. Geotechnol. 28 (3), 192–206.
Usui, A., Someya, M., 1997. Distribution and composition of marine hydrogenetic and hydrothermal manganese deposits in the Northwest Pacific. Manganese mineralization: geochemistry and mineralogy of terrestrial and marine deposits. Geol. Soc. Lond. Spec. Publ. 119, 177–198.
Usui, A., Iizasa, K., Tanahashi, M., 1994. Marine Polymetallic Mineral Deposits in the Vicinity of the Japanese Island, NW Pacific. Miscellaneous Map Ser. no. 33Geological Survey of Japan, 2 Sheet Map.
Usui, A., Graham, L.J., Ditchburn, R.G., Zondervan, A., Shibasaki, H., Hishida, H., 2007. Growth history and formation environments of ferromanganese deposits on the Philippine Sea Plate, northwestern Pacific Ocean. Island Arc 16 (3), 420–430.
Usui, A., Tanaka, M., Thornton, B., Tokumasu, A., Urabe, T., 2011. Small-scale ROV mapping of the ferromanganese crusts over the seamounts in the NW Pacific. Technical Papers: 1–4. Oceans11-MTS/IEEE Kona.
Usui, A., Sato, H., Nishi, K., Graham, I., Thornton, B., Okamoto, N., Urabe, T., 2013. Geological characterization of Co-rich ferromanganese crusts over the northwestern Pacific seamounts. Proc. Oceans 2013, San Diego (ISBN: 978-0-933957-40-4).
von Blanckenburg, F., Bouchez, J., 2014. River fluxes to the sea from the ocean's ^{10}Be/^{9}Be ratio. Earth Planet. Sci. Lett. 387, 34–44.
Vonderhaar, D.L., McMurtry, G.M., Garbe-Schoenberg, D., Stueben, D., Esser, B.K., 2000. Platinum and other related element enrichments in Pacific ferromanganese crust deposits. Marine Authigenesis: From Global to Microbial. SEPM, pp. 287–308.
Wen, X., De Carlo, E.H., Li, Y.H., 1997. Interelement relationships in ferromanganese crusts from the central Pacific Ocean: the implications for crust genesis. Mar. Geol. 136, 277–297.
Winterer, E.L., Natland, J.H., van Waasbergen, R.J., Duncan, R.A., McNutt, M.K., Wolfe, C.J., Premoli, et al., 1993. Cretaceous guyots in the NW Pacific. The Mesozoic Pacific: Geology, Tectonics, and Volcanism. AGU Geophysical Monograph 77, pp. 77–103.
Xiangwen, R., Glasby, G.P., Jihua, L., Xuefa, S., Jingwu, Y., 2007. Fine-scale compositional variations in a Co-rich Mn crust from the Marcus-Wake Seamount cluster in the western Pacific based on electron microprobe analysis (EMPA). Mar. Geophys. Res. 28, 165–182.
Yamaoka, K., Ma, L., Hishikawa, K., Usui, A., 2017. Geochemistry and U-series Dating of Holocene and Fossiel Marine Hydrothermal Manganese Deposits from the Izu-Ogasawara Arc. Ore Geol. Rev. 87, 114–125 (in this volume).